The influence of deposition parameters on structural, optical and electrical properties of *AZO* thin film

E. CHIȚANU*

National Institute for Research and Development in Electrical Engineering ICPE-CA, 313 Splaiul Unirii, 030138, Bucharest, Romania

Al-doped ZnO (*AZO*) thin films were obtained by *RF* magnetron sputtering deposition on the glass substrate, using a ceramic target (not sintered) $ZnO:Al_2O_3$ (98:2 wt. %) and *RF* powers between 100 W and 200 W, with a step of 50 W. The *AZO* films were characterized by structural, optical and electrical investigations. The *XRD* pattern indicates the presence of single phase with hexagonal crystalline structure of ZnO. The *AZO* thin film obtained by using 200 W deposition power exhibited the best *TCO* electrical and optical properties, reaching electrical resistivity of $1.20 \cdot 10^{-3}$ Ω·cm, charge mobility of 12.6 cm^2/Vs and 85% transparency in visible range.

1. Introduction

The development of the world electronics industry it was made considering the areas characteristic of modern man. A large part of the world's population uses equipments and devices that have in their composition transparent conductive oxide materials (*TCO*): portable electronics (smart phones, notebooks), monitors, flexible electronics, photovoltaic cells. In recent years, the *TCO* market has grown, reaching USD 4.5 billion in 2020 and is expected to maintain this trend in the coming years, and reach USD 10.2 billion in 2028 [1].

Special attention to *TCO* materials has led to an intense scientific activity, carried out in recent years, having as main object these materials. Due to intensive research were resulted new n-type materials [2, 3], synthesis of p-type materials [4, 5], *TCO* based on carbonic materials [6 - 8], composites materials [9, 10] and hybrid ZnO/3D graphene structures [11], but also increasing of the knowledge amount and estimating the behavior of these materials.

Thin films *TCO* materials are deposited by a variety of methods, of which can be mentioned: physical methods (sputtering [12], thermal evaporation [13], pulse laser deposition [14], magnetron sputtering [15, 16]) and chemical methods (plasma enhanced chemical vapor deposition - *PECVD* [17], low pressure chemical vapor deposition - *LPCVD* [17], metal organic chemical vapor deposition - *MOCVD* [18]). In addition to these conventional techniques, have been developed chemical solution based methods (printing [19], spin coating [20], spray pyrolysis [21]).

In recent years, ZnO-based *TCO* materials [22-25] have aroused the interest of researchers due to its remarkable property for applications in optoelectronics. Due to this attention, studies and researches have been carried out to obtain thin films with optimal electrical and optical properties for *TCO* applications. By doping with elements from group III (Al [26], Ga [27] and In [28]) was observed the enhancement of these properties and improvement of thermal stability at higher temperatures.

Aluminium-doped ZnO (*AZO*) films are a good candidate for *TCO* thin films, due to their high optical transmission, relatively low resistivity, cheap materials, non-toxicity and good stability in hydrogen plasma, compared to SnO_2-doped In_2O_3 (*ITO*) films [29] and SnO_2 doped with F (*FTO*) films [30].

The major problem for *AZO* material is the high temperature (~100ºC) required for deposition process, in order to obtain high quality films, characterized by low electrical resistivity, high optical transmission and homogeneity. As the deposition temperature decreases, the quality of thin films decreases too. Understanding the relationship between the deposition process parameters and thin film properties is very important for optimizing *AZO* thin films, in order to use in *TCO* high tech applications.

This paper aims to highlight the influence of deposition parameters (*RF* power) on the structural, electrical and optical properties of AZO thin films for their performances improvement for TCO applications.

2. Experimental

A. AZO Thin film deposition

AZO thin films were obtained by *RF* (radio frequency) magnetron sputtering method, using glass as a substrate. Glass substrates were prepared for deposition by ultrasonically cleaning with acetone, methanol and deionised water. After cleaning process, the glass substrates were dried by blowing nitrogen over them. The sputtering depositions were performed using ZnO doped

with Al_2O_3 (98:2 wt. %) target with 2-inch diameter, 15 cm distance between target and substrate, working gas Ar (15 sccm), $2 \cdot 10^{-3}$ Torr working pressure and different power ranging from 100 to 200 W, in step of 50 W.

B. Characterization

Structural analysis of films was performed by grazing incident *X*-ray diffraction employing an *X*-ray diffractometer (PANalytical's X'Pert PRO MRD). Optical analysis was performed using a double beam UV-Vis-NIR spectrophotometer [Shimadzu UV-3101 PC] for transmission spectra in the wavelength range of 300 – 2500 nm. Electrical proprieties (resistivity, mobility and carrier concentration) were determinate by Hall effect [Hall Effect System HL5500PC]. Films thickness was verified using the profillometer [XP-Plus Stylus].

3. Results and discussion

Structural properties of n-type semiconducting *AZO* films, deposited by *RF* magnetron sputtering technique, were investigated by *X*-ray diffraction. Fig. 1(*a, b, c*) shows the X-ray diffraction spectra for *AZO* thin films as functions of *RF* power (100 W, 150 W and 200 W). For all samples was obtained 2θ peak at 34.2°, corresponding to (002) plane, which implies the existence of hexagonal structures of ZnO with high crystallinity and preferential orientation on the *c*-axis. Also, peaks for Al_2O_3 or related phases cannot be observed in the spectra, which means that the aluminum replaced by substitution zinc in the hexagonal structure or segregated in a non-crystalline area on the edge of the particles [31].
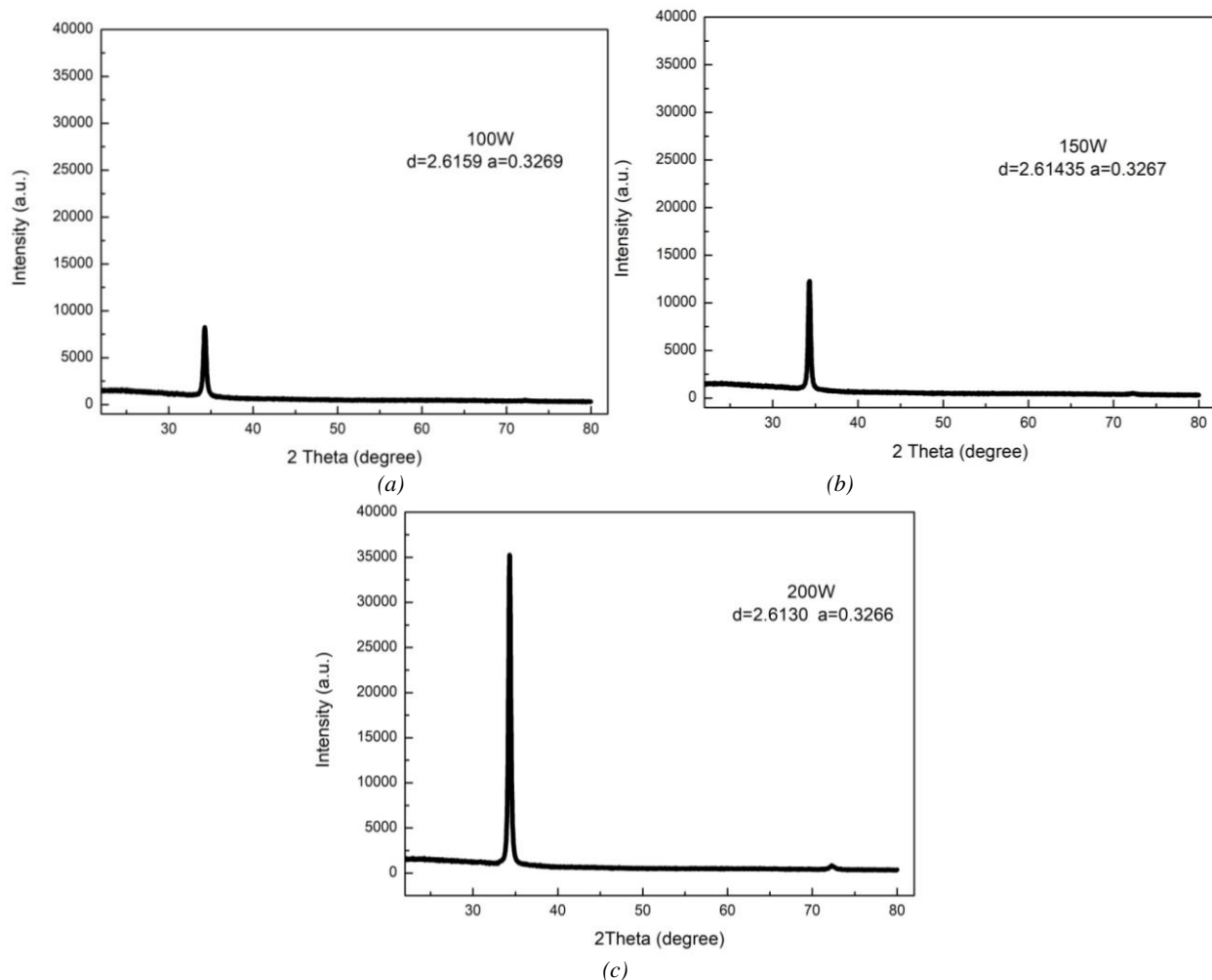

(a)

(b)

(c)

Fig. 1. The XRD pattern of AZO thin films deposited with 100 W (a), 150 W(b) and 200 W (c) RF power

In the case of the *AZO* thin film deposited with 200 W, a 2θ peak at 72.3° with low intensity can be observed, corresponding to (004) plane. The appearance of this peak can be explained through the power deposition increase; in this case, for films with the same thickness (~100 nm), the deposition rate also increases, the deposition time decreases and a small part of the atoms (0.96%) do not have enough time to develop along the (002) plane, presenting orientation on (004). However, these not influence the properties of the obtained films.

Table 1. X-ray diffraction data

Work power (W)	2θ (degree)	d (Å)	Cell parameter		Grain size (nm)	Dislocation density ($\times 10^{16}$ lines/m^2)
			a	c		
100	34.2506	2.6159	0.3269	0.5231	20.64	0.23
150	34.2723	2.6143	0.3267	0.5228	25.05	0.16
200	34.2892	2.6130	0.3266	0.5226	25.15	0.15

From XRD pattern and according to the equation (1), the lattice parameters of the unit cell were determined [32]:

$$\frac{1}{d_{2hkl}^2} = \frac{3}{4}\left(\frac{h^2 + hk + k^2}{a^2}\right) + \frac{l^2}{c^2} \qquad (1)$$

where d is the interplanar spacing, h, k, l are Miller indices and a, c cell parameters. The determinate values for the lattice parameters are also given in Table 1 (supra).

For determination of grain size (D) was used Scherrer relation (2) [33]:

$$D = \frac{0.094\lambda}{\beta \cos \theta} \qquad (2)$$

where λ (0.154 nm) is the wavelength of incident *X*-ray from *XRD*, β is the observed FWHM, measured in radians and θ is the Bragg angle of diffraction peak.

By increasing of the *RF* power, the kinetic energy of the bombarding ions will also increase, due to the momentum transfer, leading to a more efficient sputtering and thus the number of particles extracted from target will be bigger. Due to this intense bombardment, the particle size (D) increases from 20.64 nm for 100 W to 25.05 nm for 150 W and 25.15 nm for 200 W. This particle size increasing leads to a reduction in grain boundary area, considerably reducing both strain and stress in the deposited films and also the corresponding dislocation density.

The amount of defects in *AZO* thin films was estimated through dislocation density (δ), calculated using the relation (3) [34]:

$$\delta = \frac{1}{D^2} \qquad (3)$$

The small calculated values for dislocation density between $0.23 \cdot 10^{-16}$ lines/m^2 for 100 W, $0.16 \cdot 10^{-16}$ lines/m^2 for 150 W, with a minimum of $0.15 \cdot 10^{-16}$ lines/m^2 for 200 W demonstrate that *AZO* films present a good crystallinity with very small amount of defects in the crystal structure.

AZO thin films optical transmission spectra were shown in Fig. 2. In ultraviolet domain $(300 - 400$ nm), all *AZO* films show a linear increase. This sudden transition is related to the ZnO band gap, around 3.4 eV [36], if the energy of the incident light is higher than energy of the band gap of ZnO, it is absorbed quickly, otherwise it is

transmitted through the *AZO* film. As the concentration of charge carriers in the *AZO* increases, the absorption is shifted to longer wavelengths [35, 36]. In visible range (400-800 nm), samples show a high transmission, 84.22% for 100 W, 84.77 for 150 W and 85.33% for 200 W.
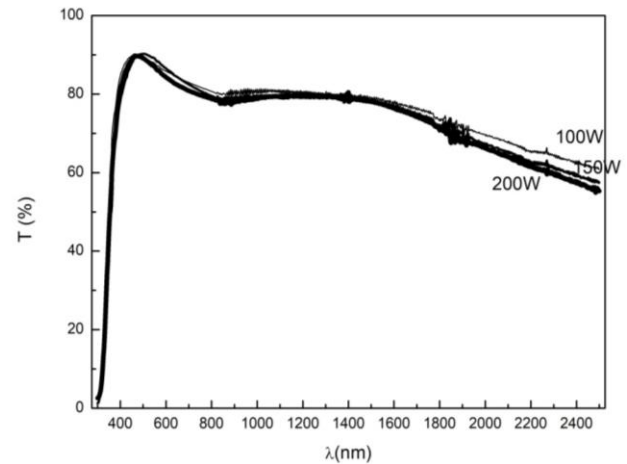

Fig. 2. The transmission variation with RF power deposition for AZO thin films

In near infrared, (800-1000 nm) the optical transmission for all samples begins to decrease due to increased photon absorption by charge carriers. This decrease is continued in the infrared domain (1000-2500 nm). This decrease in optical transmission in the *IR* range is caused by a stronger absorption of photons, due to high concentrations of charge carriers, which is confirmed by electrical measurements [37]. From the obtained results we can say that the deposition parameters influence the structural and the optical properties, the increase of *RF* power used for deposition improving these properties.

The electrical resistivity (ρ), mobility (μ) and carrier concentration (n) as function of *RF* power for *AZO* films are shown in Fig. 3. The *AZO* films show a decrease in resistivity with increasing of *RF* power: $2.85 \cdot 10^{-3}$ $\Omega \cdot$cm for 100 W, $1.45 \cdot 10^{-3}$ $\Omega \cdot$cm for 150 W and $1.2 \cdot 10^{-3}$ $\Omega \cdot$cm for 200 W. The resistivity of films depends on the *RF* power, this can be associated with changes in the ZnO crystalline structure, results confirmed by X-ray diffraction analysis. The intensity of the peak related to the (002) plane increases with RF power, while its shape does not change significantly, indicating o good crystallinity. Also, a reduction in grain boundary area induced by deposition parameters results in decreased resistivity and increased load carrier mobility [38].

Mobility and carrier concentration show an increase with the increase of the *RF* power (Fig. 3). According to optical and electrical properties, it was confirmed that *AZO* films deposited with highest power present the highest absorption in the *IR* domain.

According to study, the *AZO* film that fulfills the requirements for *TCO* (in agreement with literature) was the one deposited with highest *RF* power, 200W with good crystallinity, optical transmission in the visible range of

85.33%, resistivity $1.2 \cdot 10^{-3}$ $\Omega \cdot$cm, mobility 12.6 cm^2/Vs and carrier concentration value $4.34 \cdot 10^{20}$ cm^{-3}.
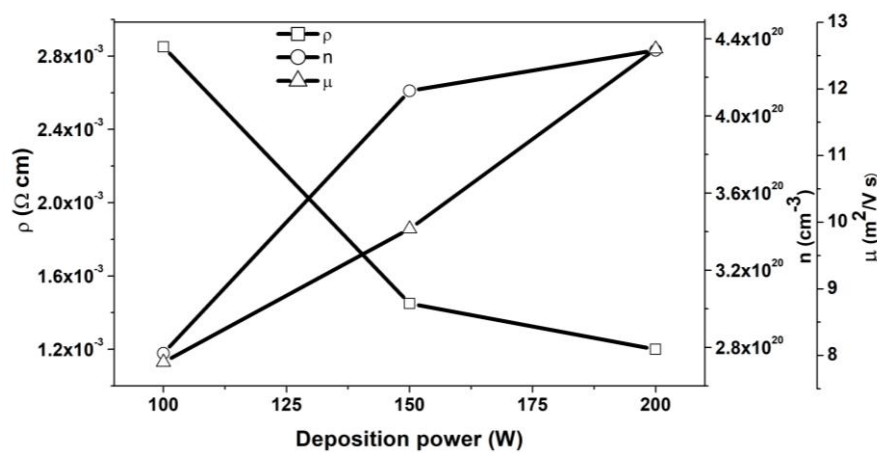

Fig. 3. The AZO films electrical resistivity (ρ), mobility (μ) and carrier concentration (n) as a function of RF power deposition

For the use of *AZO* thin films in photovoltaic cells, they must have a high optical transmission in the visible range and a low electrical resistance. These parameters are correlated in the figure of merit (*FOM*), [39] which represents performance of *TCO* materials:

$$FOM = -1/(\rho \ln(T)) \qquad (4)$$

where ρ is the resistivity and T is the average transmission in the wavelength range of $400 - 800$ nm. The *FOM* values of the *AZO* sputtered at 100 W, 150 W and 200 W are 2110 Ω^{-1}cm^{-1}, 4144 Ω^{-1}cm^{-1} and 4680 Ω^{-1}cm^{-1}, respectively.

4. Conclusions

The *AZO* films were deposited by *RF* magnetron sputtering technique with a ceramic (not sintered) target, type ZnO doped with Al_2O_3 (98:2 wt. %). Thin films were deposited onto glass substrates using *RF* power (100 W, 150 W and 200 W).

The influence of *RF* power deposition on structural, optical and electrical *AZO* films were confirmed. All the samples present a single-phase hexagonal structure with a good optical transparency in visible domain up to 85%, a resistivity lower that $1.4 \cdot 10^{-3}$ $\Omega \cdot$cm and a carrier mobility up to 12.6 cm^2/Vs.

Our study shows that by adjusting the deposition process parameters of *AZO* films, can be controlled the structural properties that are strong related to the electrical and optical properties The optoelectronic properties of the *AZO* films deposited with 200 W are better in comparison with those deposited with lower power, exhibiting the bigger values of *FOM* - 4680 Ω^{-1}cm^{-1}.

References

[1] Transparent Conductive Films Market – https://www.globenewswire.com/news-release/2020/08/26/2083764/0/en/Transparent-Conductive-Films-Market-Is-Anticipated-To-Reach-USD-10-2-Billion-By-2028.html
[2] F. Yang, X. Zhou, N. T. Plymale, K. Sun, N. S. Lewis, J. Mater. Chem. A **8**, 13955 (2020).
[3] D. Zhao, J. Li, S. Sathasivam, C. J. Carmalt, RSC Adv. **10**, 34527 (2020).
[4] L. Ben Amor, B. Belgacem, J. S. Filhol, M. L. Doublet, M. Ben Yahia, R. Ben Hassen, Chem. Commun. **56**, 2566 (2020).
[5] Y. Yin, Y. Wu, G. Chen, W. J. Yin, J. Appl. Phys. **127**, 175703 (2020).
[6] W. Prachamon, S. Limpijumnong, S. Komin, Physica E Low Dimens. Syst. Nanostruct. **124**, 114306 (2020).
[7] P. M. Rajanna, H. Meddeb, O. Sergeev, A. P. Tsapenko, S. Bereznev, M. Vehse, O. Volobujeva, M. Danilson, P. D. Lund, A. G. Nasibulin, Nano Energy **67**, 104183 (2020).

[8] A. B. Suriani, Muqoyyanah, A. Mohamed, S. Alfarisa, M. H. Mamat, M. K. Ahmad, M. D. Birowosuto, T. Soga Bull Mater Sci. **43**, 310 (2020).

[9] A. M. Darwish, S. S. Sarkisov, K. Cho, A. Giri, D. N. Patel, A. S. Sarkisov, S. Wilson, J. Wilson, J. Mathew, E. Collins, T. Welch, B. Smith, B. Koplitz, X. Zhang, Proceedings 11281, Oxide-based Materials and Devices XI; 1128118 (2020) SPIE OPTO, (2020).

[10] K. Wang, Y. Jin, B. Qian, J. Wang, F. Xiao, J. Mater. Chem. C **8**, 4372 (2020).

[11] E. Chitanu, C. Banciu, G. Sbarcea, V. Marinescu, A. Bara, P. Barbu (Prioteasa), Rev. Chim. **69**, 3376 (2018).

[12] E. P. da Silva, M. Chaves, S. F. Durrant, P. N. Lisboa-Filho, J. R. R. Bortoleto, Materials Research **17**(6), 1384 (2014).

[13] F. K. Mugwanga, P. K. Karimi, W. K. Njoroge, O. Omayio Mugwang, J. Fundam. Renewable Energy Appl. **5**, 4 (2015).

[14] S. L. Ou, D. S. Wuu, S. P. Liu, Y. C. Fu, S. C. Huang, R. H. Horng, Opt. Express **19**, 16244 (2011).

[15] F. Z. Hao, J. H. Tao, Y. Guo, C. Ma, F. Shi, Z. Hu, J. Chu, Optoelectron. Adv. Mat. **13**(3-4), 249 (2019).

[16] Q. F. Chen, Y. Y. Li, P. Y. Ying, T. L. Wang, P. Zhang, J. B. Wu, M. Huang, Y. H. Fang, V. Levchenko, Optoelectron. Adv. Mat. **14**(9-10), 427 (2020).

[17] X. Niu, M. Wang, C. Yu, B. Cheng, S. F. Liu, J. Rong, X. Mei, W. Han, J. Mao, X. Wang, S. Y. Liu, L. Li, L. Ding, L. Yang, Z. Chou, C. R. Wronski, 2013 IEEE 39th Photovoltaic Specialists Conference (PVSC), Tampa, FL, 1366 (2013).

[18] C. H. Lee, D. W. Kim, J. Electroceram. **33**, 12 (2014).

[19] K. Vernieuwe, J. Feys, D. Cuypers, K. De Buysser J. Am. Ceram. Soc. **99**(4), 1353 (2015).

[20] J. Zhang, K. Nakamura, Materials Research Innovations **18**, S4-674 (2014).

[21] Z. Amara, M. Khadraoui, R. Miloua, M. N. Amroun, K. Sahraoui, J. Optoelectron. Adv. M. **22**(3-4), 163 (2020).

[22] A. Mallick, S. Ghosh, D. Basak, Mater. Sci. Semicond. Process **119**, 105240 (2020).

[23] L. Karmakar, D. Das, Sol. Energy Mater Sol. Cells **206**, 110278 (2020).

[24] Z. Yan, J. Bao, X. Y. Yue, X. L. Li, Y. N. Zhou, X. J. Wu, J. Alloys Compd. **812**, 152093 (2020).

[25] D. Das, L. Karmakar, J. Alloys Compd. **824**, 153902 (2020).

[26] N. Kumar, A. H. Chowdhury, B. Bahrami, M. Reza Khan, Q. Qiao, M. Kumar, Thin Solid Films **700**, 137916 (2020).

[27] S. Atiq, M. T. Ansar, A. Hassan, S. K. Abbas, T. Iqbal, M. Aslam, M. J. Iqbal, A. Mahmood, Superlattices Microstruct. **144**, 106576 (2020).

[28] K. Ghosh, R. K. Pandey, Appl. Phys. A **125**, 98 (2019).

[29] S. Abbas, D. K. Ban, J. Kim, Sens. Actuator A Phys. **293**, 215 (2019).

[30] M. H. Jo, B. R. Koo, H. J. Ahn, Ceram. Int. **46,** 25066 (2020).

[31] F. Atay, V. Bilgin, I. Akyuz, S. Kose, Mater Sci. Semicond. Process **6**, 197 (2003).

[32] S. S. Lin, J. L. Huang and P. Šajgalik, Surf. Coat. Technol. **185**, 254 (2004).

[33] V. Bilgin, S. Kose, F. Atay, I. Akyuz, Mater. Chem. Phys. **94**, 13 (2005).

[34] S. A. Khalate, R. J. Deokate, R. Kate, Superlattices Microstruct. **103**, 335 (2017).

[35] B. E. Sernelius, K. Berggren, Z. Jin, I. Hamberg, C. G. Granqvist, Phys. Rev. B **37**, 10244 (1988).

[36] J. Owen, Schriften des Forschungszentrums Jülich Reihe Energie & Umwelt / Energy & Environment Band **125**, 187 (2011).

[37] M. Berginski, J. Hupkes, M. Schulte, G. Schope, H. Stiebig, B. Rech, M. Wuttig, Jpn. J. Appl. Phys. **101**, 074903 (2007).

[38] D. H. Zhang, H. L. Ma, Applied Physics A **62**, 487 (1996).

[39] S. Fernández, A. Martínez-Steele, J. J. Gandía, F. B. Naranjo, Thin Solid Films **517**(10), 3152 (2009).

_____

*Corresponding author: elena.chitanu@icpe-ca.ro